Authors accepted manuscript
Article published online: January 04, 2021 in *Structures and Buildings*
Available at DOI 10.1680/jstbu.20.00111

Effect of concrete workability on bond properties of steel rebar in pre-cracked concrete

Seyed Sina Mousavi [*1], Lotfi Guizani [1], Chandrasekhar Bhojaraju [1], and Claudiane M. Ouellet-Plamondon [1]

Abstract

Although previous research has shown a considerable influence of the pre-cracking phenomenon on steel-congested concrete members, only normal concrete (NC) has been considered in the literature. Hence, this paper intends to study the effect of the pre-cracking phenomenon on the bond response of pre-cracked NC with different slump flow values and self-consolidating concrete (SCC). Initial crack widths ranging from 0.0 to 0.5 mm are studied. Results show that initial crack widths larger than 0.10 mm have a significant influence on bond properties so that higher than 30% and 50% reduction factors are obtained for the maximum bond strength of concrete specimens exposed to the initial crack widths of 0.2 mm and 0.4 mm respectively. Results show that concrete mixtures with higher workability are less sensitive to the pre-cracking phenomenon as compared to NC mixtures. The average bond stress of steel rebar in the pre-cracked SCC is found to be similar to that of the NC with a slump flow of 200 mm, which is considerably better than for NC

[1] Dept. of Construction Engineering, Univ. of Quebec, École de technologie supérieure (ÉTS Montréal), 1100 Notre-Dame West, Montreal, QC, H3C 1K3, Canada

* Corresponding author. E-mail address: seyed-sina.mousavi-ojarestaghi.1@ens.etsmtl.ca

with a slump flow of 97 mm. Moreover, results show that 65.8%, 80.6%, 88.5%, and 93.1% fracture energy reductions are obtained for crack widths of 0.15, 0.20, 0.30, 0.40, and 0.50 mm respectively.

Keywords: bond-slip; self-consolidating concrete; pre-cracked concrete; steel rebar; flowability.

1. Introduction

Recently, there has been a growing tendency of studying bond characteristics of steel rebar embedded in cracked concrete, denoted as "pre-cracking phenomena", in which induced initial cracks generate and propagate through a plane containing a reinforcing bar (rebar) axis (Mousavi et al., 2019, Brantschen et al., 2016, Lindorf, 2011, Matsumoto et al., 2016, Mousavi et al., 2020b). Plastic shrinkage cracking in the steel-congested concrete region (Hadidi and Saadeghvaziri, 2005, Saadeghvaziri and Hadidi, 2005) and accidental internal damages due to the previous overloading (such as earthquakes and/or overstress situations) (Matsumoto et al., 2016) can cause the pre-cracking phenomenon, where corrosion plays no direct role in generating the internal crack. Until now, different expressions have been used in the literature for describing the pre-cracking phenomenon including mechanical pre-loading (Brantschen et al., 2016, Brantschen, 2016), biaxial load transfer (Lindorf et al., 2009, Saadeghvaziri and Hadidi, 2005), multiaxial stress states (Purainer, 2005), and transverse tension (Lindorf, 2011). These situations cause the crack propagation parallel to the rebar direction, resulting in internal damages at the rebar-concrete interface.

Recently, Brantschen et al. (2016) conducted an experimental investigation to study the bond behavior of steel rebar in the pre-cracked concrete by inducing initial cracks with different widths ranging from 0.20 mm to 2.0 mm. They showed that in-plane cracking has a significant effect on the bond strength along with the bond-slip stiffness. Moreover, they used the aggregate interlock approach to present an analytical model of the effect of the in-plane cracking on bond behavior. However, they reported that the bond index, in its current form, could not adequately characterize bond properties in the pre-cracked concrete. They recommended the use of rebar rib geometry (rib orientation, height, and spacing) for future studies related to the pre-cracking phenomenon (Brantschen et al., 2016). In this field, Mousavi et al. (2019) presented a specific bond-slip model and also development length formulation for predicting bond characteristic of steel rebar embedded in pre-cracked NC. They considered initial crack widths ranging from 0.10 mm to 0.40 mm in their formulations. Recently, Mousavi et al. (2020a) proposed a simplified model for bond-slip response in pre-cracked NC. They used rebar deformations (rib height and spacing) and crack width to introduce an analytical model for predicting the maximum bond strength of rebar embedded in the pre-cracked concrete. They showed that the pre-cracking phenomenon reduces the lateral concrete confinement surrounding the rebar.

As reported in previous research, steel-congested concrete members have been mostly affected by the pre-cracking phenomenon (Matsumoto et al., 2016) including the typical surface crack pattern of a slab specimen reinforced with transverse elements (cracks in punching area around column) (Brantschen et al., 2016), flexural reinforcement in slabs (Dawood and Marzouk, 2012), and reinforced concrete (RC) beam-column joints (Joergensen and Hoang, 2015). However, only NC has been considered in previous studies, while relatively new concrete generations have been introduced for using in the steel-congested regions to maintain desired structural behavior, such as

NC mixture with a slump flow value higher than 150 mm and SCC mixture with a slump flow value higher than 500 mm (Mousavi et al., 2016, Mousavi et al., 2017).

Few studies have investigated the effect of concrete workability on mechanical properties of RC members especially bond strength. They reported some conflicting results, which require further investigation. Increasing the amount of water, adding different types of superplasticizer, using a high amount of fine aggregates, using air-entraining (AE) admixture, and replacing some percentage of cement by mineral fillers are different approaches used for increasing the workability of concrete mixtures. Previous studies have focused mainly on the "top bar effect" in which using concrete mixture with a high slump flow increases the risk of the bleeding phenomenon. This increases the concrete cracking and the porosity of the hydrated cement paste surrounding the lower parts of horizontally placed rebar (Khayat and Guizani, 1997). However, despite the "top bar effect", few studies have determined the effect of concrete workability on normally-positioned rebar without the bleeding phenomenon. In this field, Collepardi and Corradi (1979) reported that the addition of chemical admixtures (naphthalene-sulfonated polymer-based superplasticizers) improves the rebar-concrete bond strength for both ordinary and lightweight mixtures along with the flowability of concrete mixtures. Similarly, Fu and Chung (1998) and Pop et al. (2015) reported that with an increase in the fluidity of concrete mixture, the interfacial void content decreases causing higher bond strength. However, Brettmann et al. (1986) showed that a high slump NC made with a high-range water-reducer (HRWR) has a lower bond strength as compared to a low slump concrete with the same compressive strength. In this field, Zilveti et al. (1985) reported that a high slump concrete mixture has comparable bond properties to those of low slump mixtures, which was confirmed by Thrane et al. (2010). However, only uncracked concrete specimens were considered in the literature.

Hence, the present study intends to determine the effect of concrete workability (or flowability) on the bond response of steel rebar embedded in pre-cracked concrete. To address this issue, an experimental program was conducted in the present study. Three different concrete mixtures with different slump values were considered for this experimental program. Bond responses of uncracked and pre-cracked specimens were studied through pull-out tests. A comparison study was also performed between the concrete mixtures with normal, medium, and high workability.

2. Experimental program

2.1 Materials

Three different concrete mixes were considered for this experimental program (Table 1). Cement was a general use Portland cement (CSA A3001 type GU or ASTM C150 type I) with a density of 3.15 g/cm^3. The fine aggregate was natural sand with a maximum grain size of 1.25 mm and a specific gravity of 2.68. The coarse aggregate was crushed gravel with a particular gravity of 2.68 and a nominal maximum diameter of 14 mm and 20 mm for normal (NC) and self-consolidating concrete (SCC) respectively. Limestone powder was used as a filler in SCC mixtures with a relative density of 2.68 and a maximum particle size of about 200 μm. The particle size distribution of the cement and limestone powder is illustrated in Fig. 1. Fresh properties and compressive strength of mixtures are given in Table 1. NC1, NC2, and SCC mixtures correspond to NC with a slump flow of 97 mm, moderate flowable NC with a slump flow of 200 mm, and SCC with a slump flow of 709 mm respectively. Water-to-total powder ratios of 0.41, 0.43, and 0.41 were considered for NC1, NC2, and SCC mixtures respectively.

2.2 Specimens and test set-ups

For each mixture, 3 cylindrical specimens with a diameter of 100 mm and a height of 200 mm were prepared to measure the concrete compressive strength. A total number of 26 cylindrical specimens with a diameter of 150 mm and a height of 113 mm were also considered for pull-out tests under monotonic loading including 9 uncracked and 17 pre-cracked specimens (Fig. 2(a)). All specimens were cured for 28 days in a moisture room at 97.3% relative humidity (RH) and 23 ºC temperature. To simulate the pre-cracking phenomenon, an indirect tensile test (Brazilian splitting test) was considered for generating cracks perpendicular to the direction of the rebar placed at the center of cylindrical specimens (Fig. 2(b)). A displacement-controlled loading with a rate of 0.15 mm/min was applied to prevent unexpected splitting failure during the pre-cracking loading. To measure the initial crack width, two crack gauges were installed at both sides of concrete cylinders. As crack width changes with unloading, the ultimate initial crack width was directly measured after stopping the pre-cracking procedure (Fig. 2(c)). Direct pull-out tests were carried out by applying tensile force directly to the rebar. An MTS testing machine with a load capacity of 250 kN was used to apply the tensile load through a displacement-controlled protocol at the rate of 0.5 mm/min. The unloaded end slip was measured with a linear variable differential transformer (LVDT). To provide a relatively uniform distribution of bond stresses, the embedment length of the rebar was 50 mm (five times the nominal diameter of rebar) in all specimens. This short-embedded length provides a better measurement of the local bond stress. Plastic sleeves were used for covering the unbonded length (Fig. 2(a)). An automatic data acquisition system was used to record the data. Crack opening during the pull-out test was also measured by crack gauges for obtaining bond stress-crack opening curves. This curve is used to obtain the bond fracture energy.

It was tried to impede the splitting bond failure in uncracked specimens by providing enough concrete cover around the rebar ($c_c/d_b = 7.5$). In all cases, the rebar was positioned at the center of cylinders. The used steel rebar has a nominal diameter of 10 mm with a specified yield strength and ultimate tensile strength of 432 MPa and 620 MPa respectively. The surface characteristics and rib pattern of the steel rebar used are shown in Fig. 2(d). The average value of rib–face angle for rebar used in the experimental program was about 55 degrees. The rib spacing-to-rib height ratio (S_r/h_r) was about 7.0.

3. Experimental results

As mentioned widely in the literature (Guizani et al., 2017, Wu and Zhao, 2012), for the short bond region (generally five times the rebar diameter), bond stress is close to uniform distribution and can be averaged along the anchorage length to get a close estimate of the local bond stress. Hence, the local bond stress, τ (N/mm^2), can be calculated by Eq. (1):

$$\tau = \frac{F}{\pi d_b l_e} \tag{1}$$

where F is the tensile load, d_b is the rebar diameter, and l_e is the embedded length. As recommended by RILEM (TC, 1994), arithmetic mean of bond stresses (denoted as "average bond stress") is calculated by Eq. (2), in which variables $\tau_{0.01}$, $\tau_{0.10}$, and $\tau_{1.00}$ corresponding to bond stresses at slips of 0.01 mm, 0.10 mm, 1.0 mm respectively.

$$\tau_m = \frac{\tau_{0.01} + \tau_{0.10} + \tau_{1.00}}{3} \tag{2}$$

Based on the literature (Trezos et al., 2014, Mousavi et al., 2019), maximum (or ultimate) bond strength (τ_u), average bond stress (τ_m), residual bond strength corresponding to a slip of 10.0 mm

(τ_r), and area under the bond-slip curve (denoted as bond energy, E_b) are considered as representative variables of bond characteristics of mixtures. All representative bond parameters are normalized to the square root of the concrete compressive strength of each mixture, $\tau/\sqrt{f'_c}$. Overall, results of uncracked and pre-cracked concrete, as well as the failure modes, are summarized in Table 2. Initial crack widths ranging from 0.0 (uncracked) to 0.5 mm were obtained by the pre-cracking tests. Specimens are designated by the type of concrete (NC1, NC2, and SCC) followed by the letter "C" and initial crack width in mm for pre-cracked concrete, or only "U" for uncracked concrete. Although three specimens were considered for every initial crack width, only two repetitions were obtained in some cases due to the brittle nature of the pre-cracking test and to the difficulty of controlling the target initial crack width. The pull-out failure mode was observed for uncracked specimens (Fig. 3(a)). Similarly, pre-cracked specimens with initial crack widths smaller than 0.15 mm ($w <$ 0.15 mm) failed by pulling out the rebar without splitting the surrounding concrete. Similar results for NC mixtures were reported by Mousavi et al. (2019), in which small initial crack width has no impact on bond failure mechanism. However, large initial crack widths significantly affect the maximum bond strength along with the failure mode so that the splitting failure mode was obtained for pre-cracked specimens with $w \geq 0.15\ mm$ (Fig. 3(b)).

3.1 Uncracked concrete

Bond-slip curves of uncracked specimens for different concrete mixtures along with the normalized bond properties are illustrated in Fig. 4(a). Although comparable results are obtained for the normalized average bond stress, general results indicate that NC2 mixture has the highest interfacial maximum bond strength and NC1 mixture has the lowest values among the other mixtures (Fig. 4(b)). Comparing mixtures with the same average bond stress (τ_m), as recommended by RILEM, is appropriate in the section of pre-cracked concrete as this parameter is meaningful notably about on both bond strength and the initial stiffness. Although SCC and NC2 mixtures have an approximately similar compressive strengths of 38.80 MPa and 40.34 MPa respectively (Table 1), SCC mixture has lower bond properties as compared to NC2 mixture. However, the maximum and residual bond strengths of SCC mixture are higher than NC1 mixture with the same water-to-powder ratio of 0.41. Many studies have reported the higher maximum bond strength of steel rebar in SCC than NC (Mousavi et al., 2017, de Almeida Filho et al., 2008, Valcuende and Parra, 2009, Sabău et al., 2016, Zhu et al., 2004, Desnerck et al., 2010), while some studies have shown comparable or slightly lower results (Esfahani et al., 2008, Castel et al., 2006, Pandurangan et al., 2010, König et al., 2001, Schiessl and Zilch, 2001, Gibbs and Zhu, 1999, Lorrain and Daoud, 2002). These observed inconsistency of the test results may attributed to the concrete compositions and the experimental conditions considered in the literature (Sfikas and Trezos, 2013).

3.2 Pre-cracked concrete

Bond-slip curves of pre-cracked specimens for the studied concrete mixtures are shown in Fig. 5. General results show that the pre-cracking phenomenon has a significant impact on the bond-slip curve so that a high reduction is observed for the bond energy in pre-cracked concrete. In the case of uncracked concrete, there is a plateau after the maximum bond strength, while a sudden drop is observed for pre-cracked concrete in all mixtures. As the initial crack width increases, the slope of the descending branch of the bond-slip curve increases, which shows a more rapid drop in bond stress with increasing slip (Fig. 5). Although specimens with small initial crack widths ($w < 0.15$

mm) have similar plateau at the peak, the pre-cracking phenomenon affects the post-peak bond response so that the slope of the descending branch of the bond-slip curve is steeper as compared to uncracked concrete (Fig. 5(a, c)). This leads to about 39.0% and 42.0% reductions in the area under the bond-slip curves (characteristic bond energy, E_b) (Table 2). A low characteristic energy value corresponds to the brittle bond behavior, while a high energy value results from a ductile bond response (Mousavi et al., 2019).

To determine the bond strength reduction due to the pre-cracking phenomenon, a reduction factor is defined as below:

$$RF = \left[\frac{\tau_{Uncracked} - \tau_{Pre-cracked}}{\tau_{Uncracked}}\right] \times 100 \qquad (3)$$

where $\tau_{Uncracked}$ and $\tau_{Pre-cracked}$ are bond strengths of uncracked and pre-cracked concrete respectively, which are listed in Table 2. Reduction factors corresponding to the maximum bond strength of mixtures are illustrated in Fig. 6(a). Results show that SCC mixture has the lowest reduction factor among the other mixtures which indicate that, in terms of the maximum bond strength, SCC mixture is less sensitive to the pre-cracking phenomenon than NC mixture. This can be attributed to the high paste content in SCC mixture as compared to NC mixture. Regarding NC mixtures, as slump flow value increases, the sensitivity of concrete to the pre-cracking phenomenon decreases, so that NC2 has a lower reduction factor as compared to NC1 for the maximum bond strength. Regarding uncracked concrete, Fu and Chung (1998) and Pop et al. (2015) reported that with an increase in the slump (fluidity) of concrete mixture, the interfacial microvoids around the rebar decreases causing a higher bond strength. Uniform distribution of matrix and aggregate surrounding the rebar, due to the higher slump of concrete, may increase the probability of the aggregate interlocking phenomenon across the initial cracks. This phenomenon causes an increase in the maximum bond strength and average bond stress of high slump flow mixtures. As shown in Fig. 6(a), the reduction factor of the bond strength has a good empirical correlation with the initial crack width (w) for all mixtures as follows:

$$RF_{NC1} = 163.36w \qquad R^2=0.99 \tag{4}$$

$$RF_{NC2} = 193.68w \qquad R^2=0.96 \tag{5}$$

$$RF_{SCC} = 138.30w \qquad R^2=0.95 \tag{6}$$

Similarly, in the case of the average bond stress, NC1 has the highest reduction factor (Fig. 6(b)), while SCC and NC2 mixtures have approximately similar reduction factor. Although there is no precise trend for the reduction factor of the residual bond strength (Fig. 6(c)), the general tendency indicates that SCC mixture has the lowest reduction factor among the other mixtures.

Regarding small initial crack widths ($w \leq 0.10$ mm), as mentioned in Table 2, the pull-out failure mode was observed for SCC specimen, while the failure was sudden for NC2 specimen causing concrete splitting along with pulling-out the rebar. As shown in Fig. 7(a), initial crack widths cause 16.92% and 5.73% maximum bond strength reductions in NC2 and SCC mixtures respectively. Similar observations are obtained for the average bond stress (τ_m) and the residual bond strength (τ_r). However, comparable bond energy (E_b) is obtained for both mixtures. Regarding the average bond stress, even improvement in bond strength is observed for pre-cracked SCC specimens as compared to the uncracked ones (Fig. 7(a)), which may be due to the aggregate interlock at the crack surfaces. Crack opening of specimens was also measured for NC2 and SCC mixtures. Two crack gauges were installed at both sides of rebar during the pull-out tests. As illustrated in Fig. 7(b), for pre-cracked SCC specimen, similar crack width opening is observed during the tests for two gauges, while different values of crack width opening are noted for NC2 mixture. Moreover, results show that an approximate linear ascending branch is observed for both mixtures prior to a plateau, before reaching the maximum bond strength. The stiffness of this initial branch of the curve is steeper for NC2 mixture specimens as compared to SCC mixture. The length of this plateau is longer for SCC mixture specimens as compared to NC2 mixture, which means that higher sustained bond strength is obtained. The area under the bond-crack opening curve demonstrates the fracture energy. Similar to the bond energy shown in Fig. 7(a), for a small initial crack width, pre-cracked SCC specimen shows slightly higher/comparable fracture energy for the ascending branch of the bond stress-crack opening curve ending at the maximum bond strength (Fig. 7(b)), as compared to NC2 specimen.

Bond stress-crack opening curves of the pre-cracked specimens with large initial crack widths are illustrated in Fig. 8. Results show that an unsymmetrical crack opening phenomenon happened during pull-out tests (Fig. 3(c)). Results presented in Fig. 8 show that this phenomenon is more crucial for NC2 specimens as compared to SCC ones, causing different bond stress-crack opening curves for two crack gauges installed at both sides of the steel rebar. The results shown in Figs. 7 and 8 indicate that the crack opening of large initial cracks is different from the small ones. Crack opening more than 6.0 mm is observed for large crack widths (Fig. 8). Crack opening is very small until the peak (maximum bond strength, τ_u), while considerable crack opening values and also sudden drops in curves are observed after the peak. Additionally, crack gauges installed at both sides of rebar show different behaviors before and after the maximum bond strength. This indicates the existence of non-uniform (or unsymmetric) crack opening surrounding the rebar after the pre-cracking phenomenon that arises mostly from the brittle nature of the cracking in concrete (Fig. 8). The area under the bond stress-crack opening curve can be used as the "fracture energy,

F_{energy}" of the bond mechanism in the pre-cracked specimen. The maximum, minimum, and average values of the fracture energy of NC2 and SCC mixtures are shown in Fig. 9, concerning the initial crack widths. Results show that as the initial crack width increases, the average fracture energy decreases so that 40.7%, 13.9%, 7.9%, and 2.8% values are obtained for fracture energies of specimens exposed to 0.15, 0.2, 0.3, 0.4, and 0.5 mm initial crack widths. Similar results are observed for the minimum and maximum values of the fracture energy. Finally, Eq. (7) is achieved for predicting the fracture bond energy of pre-cracked specimens as a function of the secondary crack opening ($\acute{w}$) with a good correlation of R^2=0.99, as follows:

$$F_{energy} = 42.45\acute{w}^{-1.62} \tag{7}$$

4. Discussion

As reported by Mousavi et al. (2019), rebar diameter has a considerable impact on the influence of the pre-cracking phenomenon, so that normalized bond stress is related to the initial crack width-to-rebar diameter ratio (w/d_b). A similar trend is illustrated in Fig. 10. NC2 and SCC mixtures approximately have the same trend, while NC1 mixture follows different trends. Good correlations exist between the experimental results and the w/d_b ratio for all mixtures, as expressed by Eqs. (8)-(10). Values of 3.41, 4.18 and 3.97 are obtained for the normalized bond strength of uncracked specimens of NC1, NC2, and SCC mixtures respectively ($w = 0$), which reduce linearly with the initial crack width as follows:

$$\left[\frac{\tau_u}{\sqrt{f'_c}}\right]_{NC1} = -73.41\frac{w}{d_b} + 3.41 \qquad R^2=0.97 \tag{8}$$

$$\left[\frac{\tau_u}{\sqrt{f'_c}}\right]_{NC2} = -77.69\frac{w}{d_b} + 4.18 \qquad R^2=0.99 \qquad (9)$$

$$\left[\frac{\tau_u}{\sqrt{f'_c}}\right]_{SCC} = -64.15\frac{w}{d_b} + 3.97 \qquad R^2=0.97 \qquad (10)$$

Based on the proposed equations for the normalized bond strength of rebar in pre-cracked concrete, existence of the initial cracks with widths of larger than 0.52 mm, 0.61 mm, and 0.70 mm results in zero bond strength ($\tau_{max}/\sqrt{f'_c} \approx 0$) for NC1, NC2, and SCC mixtures respectively. This high value of the initial crack width corresponding to SCC mixture shows a considerable resistance to the pre-cracking phenomenon. General observations show that the initial crack width significantly changes the interfacial bond behavior so that bond failure mode is changed for initial crack widths larger than 0.15 mm. The results summarized in Table 2 and Fig. 10 demonstrate that bond behavior of a pre-cracked specimen with $w \geq 0.15$ mm is governed by the splitting failure mode, where a post-peak sudden drop in bond stress can be observed until reaching an equilibrium between the radial component of the post-splitting bond stresses and the post-splitting confining action (tensile resistance of the concrete) (Harajli, 2009, Mousavi et al., 2019). This can be attributed to the change in the failure mode, which is the main objective of the following sections related to the theoretical analysis.

As reported by Murcia-Delso and Benson Shing (2014), surface separation (in both parallel and normal directions) between the rebar and the surrounding concrete plays a significant role in the bond-slip phenomenon, which can significantly affect the interface strength. Induced initial crack generated by the pre-cracking phenomenon causes similar surface separation with a more significant impact (Mousavi et al., 2020a, Mousavi et al., 2019). As comprehensively described by Mousavi et al. (2020a), the height of the rib above the surface of the rebar plays a major role in the rebar-concrete interface separation due to the pre-cracking phenomenon. Thus, the ratio of the initial crack width-to-rib height can be used to present the bond reduction factor. Murcia-Delso and Benson Shing (2014) presented a bond-slip model considering the surface separation. They related the bond strength to the rib height without concentrating on the pre-cracking phenomenon. Accordingly, a reduction factor (ρ_{nm}) can be achieved based on the obtained experimental results, as a function of the surface separation, as follows:

$$\rho_u = \frac{(\tau_u)_{\text{pre-cracked}}}{(\tau_u)_{\text{uncracked}}} \tag{11}$$

$$\rho_u = \begin{cases} 1 & w/2 \leq M_1 h_r \\ f(w/h_r) & M_1 h_r < w/2 < M_2 h_r \\ 0 & w/2 \geq M_2 h_r \end{cases} \tag{12}$$

where ρ_u is a reduction ratio of the bond strength that considers the opening of cracks due to the pre-cracking phenomenon. M_1 and M_2 are empirical coefficients for different concrete compositions, which are summarized in Table 3. As shown in Fig. 2(d), value of 1.89 mm was measured for the rib height of the steel rebar.

The performance of the proposed model is shown in Fig. 11. The dependence of the reduction ratio (ρ_u) on the ratio of the initial crack width-to-rib height (Eq. (12)) can be attributed to the fact that the loss of bond strength is related to a reduction in the interfacial contact between the steel ribs and the concrete. For a well-confined situation (uncracked concrete and $w \leq 0.10$), the interface separation is very small; consequently, the reduction factor will be equal or very close to one ($\rho_u \approx 1.0$). Different separation mechanisms can be occurred for a pre-cracked specimen, including one-side and both-side separations. The value of 0.50 is considered in this section, which corresponds to the initial crack width of $w/2$ at each side of the rebar. This value was suggested by Brantschen et al. (2016) as an idealized pre-cracking situation. Based on the experimental results (Table 3), the domain of $w/2 \leq 0.026h_r$ is obtained (for all mixtures) in the Eq. (12) for the reduction factor equal to 1.0. Based on the model presented by Murcia-Delso and Benson Shing (2014), if the interface separation is larger than the rib height, the contact between ribs and the concrete is lost, and the bond stress disappears ($\rho_u = 0$). However, the values of $0.14h_r$, $0.16h_r$, and $0.19h_r$ are obtained for NC1, NC2, and SCC mixtures respectively, as the critical separation values for a complete loss of the bond strength. These values correspond to the initial crack widths of $w \approx 0.61$, 0.52, and 0.70 mm for NC1, NC2, and SCC mixtures respectively (Figs. 6 and 10). This may be attributed to the significant reduction in the concrete compressive strength due to the pre-cracking phenomenon, which has been reported by several works (Vecchio and Collins, 1993, Kollegger and Mehlhorn, 1990, Shirai and Noguchi, 1989, Mikame et al., 1991, Belarbi and Hsu, 1991). Considerable effect of compressive strength on the rebar-concrete interfacial strength has been frequently confirmed (Guizani et al., 2017, Mousavi et al., 2017).

It is worth mentioning that the proposed equations are validated for the experimental results of the present study. More experimental investigations are necessary to determine the efficiency of the proposed equations and to generalize them for different concrete mixtures.

5. Conclusion

An experimental program was conducted in the present study to determine the effect of concrete workability (or flowability) on the pre-cracking phenomenon. Three concrete mixtures with normal, moderate, and high flowability were considered. Specimens with different initial crack widths were obtained through the Brazilian test (splitting). Pull-out results of the pre-cracked specimens were compared with the uncracked ones. According to the experimental results, the following conclusions can be drawn:

- In the case of uncracked specimens, general results show that SCC mixture has 13.2% higher normalized maximum bond strength as compared to NC1 mixture (normal concrete with a high slump flow of 97 mm) with the same water-to-powder ratio of 0.41. However, SCC mixture has 20.4% lower normalized maximum bond strength than NC2 mixture (normal concrete with slump flow of 200 mm) with approximately the same compressive strength. This trend is more significant in the normalized residual bond strength among the other interfacial bond parameters.
- Overall, results corresponding to the pre-cracked specimens show that SCC mixture is less sensitive to the pre-cracking phenomenon as compared to NC mixtures so that the slope of the maximum bond strength-crack width curves are 163.36, 193.68, and 138.30 for NC1, NC2, and SCC mixtures respectively. Moreover, in terms of the maximum bond strength and the average bond stress, NC2 mixture shows better performance (lower reduction factor) for all initial crack widths than NC1 mixture. A higher value of slump flow can be the main reason for this observation.
- Empirical equations are presented for all pre-cracked specimens (Eq. (12)). They show that despite the existing scenario of the total bond reduction until the surface clearance of $w = h_r$, values of $0.14h_r$, $0.16h_r$, and $0.19h_r$ are obtained for NC1, NC2, and SCC mixtures respectively as the critical separation values for complete loss in bond strength.
- Results of the present study indicate that more specifications should be considered in the current concrete design codes for considering the effect of the pre-existing cracks on the maximum bond strength, especially in steel-congested concrete members such as interior

and exterior joints, slabs, and shear walls. Generally, the critical initial crack width of 0.15 mm should be specified in codes to preserve the bond properties.

As various types of fillers with different dosages can be used to produce SCC mixture, more experimental studies are necessary to determine the effect of the pre-cracking phenomenon on the bond of pre-cracked concrete. Also, more experimental studies are suggested for future works to comprehensively determine the performance of the proposed models for different types of concrete mixtures, various rib geometries of rebar, and transverse confinement.

Conflict of interests

The authors declare that there are no competing interests regarding the publication of this paper.

Acknowledgements

The authors would like to thank the ÉTS Montréal technical staff for support in our experiments.

List of symbols

B	length of the top horizontal and diagonal section of ribs
d_b	rebar diameter
E_b	Absorbed energy by the bond mechanism
F	tensile force of pull-out test
F_{energy}	fracture bond energy
f'_c	concrete compressive strength
h_r	rib height of rebar
l_e	embedded length ($5d_b$)
M1, M2	empirical coefficients for Eq. (11)
RF	bond properties reduction factor due to the pre-cracking phenomenon

S_r	spacing of periodical ribs
S_{r0}	effective length of crushed concrete between two adjacent ribs
w	initial crack width
$\acute{w}$	crack opening during the pull-out test of pre-cracked specimens
w/c	water-to-cement ratio
w/p	water-to-powder ratio
τ	bond stress
τ_m	average bond stress as defined by RILEM
$\tau_{0.01}$	bond stress at slip of 0.01 mm
$\tau_{0.10}$	bond stress at slip of 0.10 mm
$\tau_{1.00}$	bond stress at slip of 1.0 mm
$\tau_{Uncracked}$	bond stress for uncracked concrete
$\tau_{Pre-cracked}$	bond stress for pre-cracked concrete
τ_u	maximum bond strength
τ_r	residual bond strength
α	rib–face angle
ρ_u	bond reduction ratio as a function of rebar height and crack width

References

BELARBI, A. & HSU, T. T. C. 1991. Constitutive laws of reinforced concrete in biaxial tension-compression, Research Report UHCEE 91-2. Department of Civil & Environmental Engineering, University of Houston.

BRANTSCHEN, F. 2016. Influence of bond and anchorage conditions of the shear reinforcement on the punching strength of RC slabs.

BRANTSCHEN, F., FARIA, D., FERNÁNDEZ RUIZ, M. & MUTTONI, A. 2016. Bond behaviour of straight, hooked, U-shaped and headed bars in cracked concrete. *Structural Concrete,* 17**,** 799-810.

BRETTMANN, B. B., DARWIN, D. & DONAHEY, R. C. Bond of reinforcement to superplasticized concrete. 1986. American Concrete Institute.

CASTEL, A., VIDAL, T., VIRIYAMETANONT, K. & FRANÇOIS, R. 2006. Effect of reinforcing bar orientation and location on bond with self-consolidating concrete. *ACI Materials Journal,* 103**,** 559.

COLLEPARDI, M. & CORRADI, M. 1979. Influence of naphthalene-sulfonated polymer based Superplasticizers on the strength of ordinary and lightweight concretes. *Special Publication,* 62**,** 315-336.

DAWOOD, N. & MARZOUK, H. 2012. Cracking and tension stiffening of high-strength concrete panels. *ACI Structural Journal,* 109**,** 21.

DE ALMEIDA FILHO, F. M., MOUNIR, K. & EL DEBS, A. L. H. 2008. Bond-slip behavior of self-compacting concrete and vibrated concrete using pull-out and beam tests. *Materials and Structures,* 41**,** 1073-1089.

DESNERCK, P., DE SCHUTTER, G. & TAERWE, L. 2010. Bond behaviour of reinforcing bars in self-compacting concrete: experimental determination by using beam tests. *Materials and Structures,* 43**,** 53-62.

ESFAHANI, M. R., LACHEMI, M. & KIANOUSH, M. R. 2008. Top-bar effect of steel bars in self-consolidating concrete (SCC). *Cement and Concrete Composites,* 30**,** 52-60.

FU, X. & CHUNG, D. 1998. Effects of water-cement ratio, curing age, silica fume, polymer admixtures, steel surface treatments and corrosion on the bond between concrete and steel reinforcing bar. *Materials Journal,* 95**,** 725-734.

GIBBS, J. & ZHU, W. Strength of hardened self-compacting concrete. Proceedings of First international RILEM Symposium on Self-Compacting Concrete (PRO 7), Stockholm, Suede, 1999. 199-209.

GUIZANI, L., CHAALLAL, O. & MOUSAVI, S. S. 2017. Local bond stress-slip model for reinforced concrete joints and anchorages with moderate confinement. *Canadian Journal of Civil Engineering,* 44**,** 201-211.

HADIDI, R. & SAADEGHVAZIRI, M. A. 2005. Transverse cracking of concrete bridge decks: State-of-the-art. *Journal of Bridge Engineering,* 10**,** 503-510.

HARAJLI, M. 2009. Bond stress–slip model for steel bars in unconfined or steel, FRC, or FRP confined concrete under cyclic loading. *Journal of structural engineering,* 135**,** 509-518.

JOERGENSEN, H. B. & HOANG, L. C. 2015. Strength of loop connections between precast bridge decks loaded in combined tension and bending. *Structural Engineering International,* 25**,** 71-80.

KHAYAT, K. H. & GUIZANI, Z. 1997. Use of viscosity-modifying admixture to enhance stability of fluid concrete. *Materials Journal,* 94**,** 332-340.

KOLLEGGER, J. & MEHLHORN, G. 1990. Experimentelle Untersuchungen zur Bestimmung der Druckfestigkeit des gerissenen Stahlbetons bei einer Querzugbeanspruchung, Rep. 413. *Deutscher Ausschuß für Stahlbeton.* Deutscher Ausschuss fur Stahlbeton, Berlin, Germany.

KÖNIG, G., HOLSCHEMACHER, K., DEHN, F. & WEIBE, D. Self-compacting concrete-time development of material properties and bond behaviour. Proceeding of 2nd International RILEM Symposium on Self-Compacting Concrete (Pro 33), Tokio, Japan, 2001. 507-516.

LINDORF, A., LEMNITZER, L. & CURBACH, M. 2009. Experimental investigations on bond behaviour of reinforced concrete under transverse tension and repeated loading. *Engineering Structures,* 31**,** 1469-1476.

LINDORF, C. 2011. *Bond fatigue in reinforced concrete under transverse tension.* PhD Thesis. Dresden University.

LORRAIN, M. & DAOUD, A. 2002. Bond in self-compacting concrete. *Proceedings Bond in Concrete from research to standards***,** 529-536.

MATSUMOTO, K., WANG, T., HAYASHI, D. & NAGAI, K. 2016. Investigation on the pull-out behavior of deformed bars in cracked reinforced concrete. *Journal of Advanced Concrete Technology,* 14**,** 573-589.

MIKAME, A., UCHIDA, K. & NOGUCHI, H. A study of compressive deterioration of cracked concrete. Proceedings International Workshop on Finite Element Analysis of Reinforced Concrete, 1991.

MOUSAVI, S., DEHESTANI, M. & MOUSAVI, K. 2017. Bond strength and development length of steel bar in unconfined self-consolidating concrete. *Engineering Structures,* 131**,** 587-598.

MOUSAVI, S., DEHESTANI, M. & MOUSAVI, S. 2016. Bond strength and development length of glass fiber-reinforced polymer bar in unconfined self-consolidating concrete. *Journal of Reinforced Plastics and Composites,* 35**,** 924-941.

MOUSAVI, S. S., GUIZANI, L. & OUELLET-PLAMONDON, C. M. 2019. On bond-slip response and development length of steel bars in pre-cracked concrete. *Construction and Building Materials,* 199**,** 560-573.

MOUSAVI, S. S., GUIZANI, L. & OUELLET-PLAMONDON, C. M. 2020a. Simplified

Analytical Model for Interfacial Bond Strength of Deformed Steel Rebars Embedded in Pre-cracked Concrete. *Journal of Structural Engineering,* 146**,** 04020142.

MOUSAVI, S. S., OUELLET-PLAMONDON, C. M., GUIZANI, L., BHOJARAJU, C. & BRIAL, V. 2020b. On mitigating rebar–concrete interface damages due to the pre-cracking phenomena using superabsorbent polymers. *Construction and Building Materials,* 253**,** 119181.

MURCIA-DELSO, J. & BENSON SHING, P. 2014. Bond-slip model for detailed finite-element analysis of reinforced concrete structures. *Journal of Structural Engineering,* 141**,** 04014125.

PANDURANGAN, K., KOTHANDARAMAN, S. & SREEDARAN, D. 2010. A study on the bond strength of tension lap splices in self compacting concrete. *Materials and structures,* 43**,** 1113-1121.

POP, I., DE SCHUTTER, G., DESNERCK, P. & SZILAGY, H. 2015. Influence of self-compacting concrete fresh properties on bond to reinforcement. *Materials and Structures,* 48**,** 1875-1886.

PURAINER, R. 2005. *Last-und Verformungsverhalten von Stahlbetonflächentragwerken unter zweiaxialer Zugbeanspruchung.* Universität der Bundeswehr München, Universitätsbibliothek.

SAADEGHVAZIRI, M. A. & HADIDI, R. 2005. Transverse cracking of concrete bridge decks: effects of design factors. *Journal of Bridge Engineering,* 10**,** 511-519.

SABĂU, M., POP, I. & ONEŢ, T. 2016. Experimental study on local bond stress-slip relationship in self-compacting concrete. *Materials and Structures,* 49**,** 3693-3711.

SCHIESSL, A. & ZILCH, K. The effect of the modified composition of SCC on shear and bond behavior. Proceedings of the 2nd International Symposium on Self-Compacting Concrete, Tokyo, Japan, 2001. 501506.

SFIKAS, I. P. & TREZOS, K. G. 2013. Effect of composition variations on bond properties of self-compacting concrete specimens. *Construction and building materials,* 41**,** 252-262.

SHIRAI, N. & NOGUCHI, H. 1989. Compressive deterioration of cracked concrete. *ASCE Struct. Congress: Design, analysis, and testing.* New York: ASCE.

TC, R. 1994. RILEM recommendations for the testing and use of constructons materials, RC 6 bond test for reinforcement steel. 2. Pull-out test, 1983, E & FN SPON.

THRANE, L., PADE, C., IDZERDA, C. & KAASGAARD, M. 2010. Effect of rheology of SCC on bond strength of ribbed reinforcement Bars. *Design, Production and Placement of Self-Consolidating Concrete.* Springer.

TREZOS, K. G., SFIKAS, I. P. & ORFANOPOULOS, K. 2014. Bond of self-compacting concrete incorporating silica fume: Top-bar effect, effects of rebar distance from casting point and of rebar-to-concrete relative displacements during setting. *Construction and Building Materials,* 73**,** 378-390.

VALCUENDE, M. & PARRA, C. 2009. Bond behaviour of reinforcement in self-compacting concretes. *Construction and Building Materials,* 23**,** 162-170.

VECCHIO, F. J. & COLLINS, M. P. 1993. Compression response of cracked reinforced concrete. *Journal of structural engineering,* 119**,** 3590-3610.

WU, Y.-F. & ZHAO, X.-M. 2012. Unified bond stress–slip model for reinforced concrete. *Journal of Structural Engineering,* 139**,** 1951-1962.

ZHU, W., SONEBI, M. & BARTOS, P. 2004. Bond and interfacial properties of reinforcement in self-compacting concrete. *Materials and structures,* 37**,** 442.

ZILVETI, A., SOOI, T., KLINGNER, R., CARRASQUILLO, R. & JIRSA, J. 1985. Effect of Superplasticizers on the Bond Behavior of Reinforcing Steel in Concrete Members.

Table 1 Mixture proportions, fresh properties, and compressive strength

Constituent	Quantity (kg/m^3)		
	NC1	NC2	SCC
Water	165	170	215
Cement (GU)	395	395	420
Limestone powder	-	-	105
Fine aggregate	788	788	940
Coarse aggregate (5-10 mm)	822	822	352
Coarse aggregate (10-14 mm)	258	258	219
Coarse aggregate (14-20 mm)	-	-	270
Superplasticizer	2.34	5.2	5.0
Viscosity modifying admixture	-	-	2.5
Air entraining admixture	-	0.83	-
w/c	0.41	0.43	0.51
w/p[1]	0.41	0.43	0.41
Fresh mix temperature (ºC)	20.9	21.8	22.7
Slump (mm)	97	200	709
T_{50} (s)	-	-	2.37
Hardened density (kg/m^3)	2453.80	2390.08	2375.70
f'_c (MPa)	58.82 (1.39)	38.80 (0.95)	40.34 (0.72)

[1] water-to-powder ratio, p=weight of powder (cement+limestone).
* data inside the parentheses denote the standard deviation.

Table 2 Bond characteristics and corresponding standard deviations for mixtures

Specimens	f'_c	w	$\tau_{0.01}$	$\tau_{0.1}$	$\tau_{1.0}$	τ_m	$\tau_m/\sqrt{f'_c}$	τ_u	$\tau_u/\sqrt{f'_c}$	τ_r	$\tau_r/\sqrt{f'_c}$	E_b	Failure*
NC1-U	58.8 (1.39)	0	13.60	21.43	23.40	19.48	2.54	25.19	3.28	5.77	0.75	146.0	P
		0	5.77	16.60	23.67	15.35	2.00	25.07	3.27	5.55	0.72	147.9	P
		0	4.98	21.07	26.03	17.36	2.26	27.12	3.54	8.18	1.07	163.6	P
		average	-	-	-	17.40 (2.07)	2.27 (0.27)	25.79 (1.15)	3.36 (0.15)	6.50 (1.46)	0.85 (0.19)	152.5	-
NC1-C0.2		0.20	2.52	13.96	5.48	7.32	0.95	18.05	2.35	0.00	0.00	12.6	S
NC1-C0.3		0.30	1.59	6.94	2.25	3.59	0.47	12.87	1.68	0.66	0.09	9.1	S
		0.30	0.77	5.22	5.57	3.85	0.50	10.41	1.36	0.01	0.00	8.8	S
		average	-	-	-	3.72 (0.18)	0.49 (0.02)	11.64 (1.74)	1.52 (0.23)	0.34 (0.46)	0.05 (0.06)	8.9	-
NC1-C0.4		0.40	0.05	0.27	4.07	1.46	0.19	4.71	0.61	0.17	0.02	4.0	S
		0.40	1.26	4.51	0.00	1.92	0.25	4.51	0.59	0.00	0.00	1.1	S
		average	-	-	-	1.69 (0.33)	0.22 (0.04)	4.61 (0.14)	0.60 (0.01)	0.09 (0.12)	0.01 (0.01)	2.6	-
NC2-U	38.8 (0.95)	0	5.32	13.27	24.53	14.37	2.31	24.74	3.97	14.60	2.15	180.1	P
		0	5.65	12.54	26.06	14.75	2.37	26.68	4.28	14.25	2.29	203.3	P
		0	9.39	17.85	27.29	18.18	2.92	27.47	4.41	17.75	2.85	221	P
		average	-	-	-	15.77 (2.10)	2.53 (0.34)	26.30 (1.40)	4.22 (0.23)	15.53 (1.93)	2.43 (0.37)	201.5	-
NC2-C0.1		0.10	5.71	12.34	21.84	13.30	2.13	21.85	3.51	0.0	0.0	117.0	S-P
NC2-C0.15		0.15	3.63	8.47	17.56	9.89	1.59	18.48	2.97	0.0	0.0	82.5	S
NC2-C0.5		0.50	1.36	3.92	2.96	2.75	0.44	5.51	0.88	0.56	0.09	8.11	S
		0.50	2.20	3.92	0.87	2.33	0.37	4.09	0.66	0.09	0.01	3.47	S
		average	-	-	-	2.54 (0.30)	0.41 (0.05)	4.80 (1.00)	0.77 (0.16)	0.33 (0.33)	0.05 (0.06)	5.79	-
SCC-U	40.3 (0.72)	0	5.74	14.16	23.92	14.61	2.30	23.95	3.77	12.95	2.04	180.6	P
		0	6.24	16.59	24.59	15.81	2.49	24.71	3.89	12.17	1.92	176.7	P
		0	5.39	16.16	25.05	15.53	2.45	25.16	3.96	11.52	1.81	171.3	P
		average	-	-	-	15.32 (0.63)	2.41 (0.10)	24.61 (0.61)	3.87 (0.10)	12.21 (0.72)	1.92 (0.12)	176.2	-
SCC-C0.1		0.10	9.92	16.37	22.84	16.38	2.58	23.20	3.65	4.97	0.78	108.0	P
SCC-C0.2		0.20	2.82	10.95	7.79	7.19	1.13	18.43	2.90	0.41	0.06	16.7	S
		0.20	3.27	11.68	0.0	4.98	0.78	16.83	2.65	0.0	0.0	9.8	S
		0.20	1.33	7.43	15.69	8.15	1.28	19.68	3.10	1.66	0.26	49.3	S
		average	-	-	-	8.77 (1.63)	1.06 (0.26)	18.31 (1.43)	2.88 (0.23)	0.69 (0.86)	0.11 (0.14)	25.3	-
SCC-C0.3		0.30	0.84	7.52	0.15	2.84	0.45	15.11	2.38	0.08	0.013	5.9	S
		0.30	3.54	11.58	8.54	7.89	1.24	14.33	2.26	0.35	0.06	17.4	S
		average	-	-	-	5.37 (3.57)	0.85 (0.56)	14.72 (0.55)	2.32 (0.08)	0.22 (0.19)	0.04 (0.03)	11.7	-
SCC-C0.4		0.40	1.02	6.40	6.8	4.74	0.75	10.31	1.62	0.23	0.04	11.8	S
		0.40	4.20	9.87	1.80	5.29	0.83	9.90	1.56	0.10	0.02	7.7	S
		average	-	-	-	5.02 (0.39)	0.79 (0.06)	10.11 (0.29)	1.59 (0.04)	0.17 (0.09)	0.03 (0.01)	9.8	-

* Modes of failure: P=pull-out; S=splitting./ Note: data inside the parentheses denote the standard deviation.

Table 3 Empirical coefficients used in Eq. (6) for different concrete compositions

Mix	$f(w/h_r)$ in Eq. (6)	M_1	M_2
NC1	$f(w/h_r) = -5.11\frac{w}{h_r} + 1.26$	0.026	0.14
NC2	$f(w/h_r) = 1.41e^{(-7.79\frac{w}{h_r})}$	0.026	0.16
SCC	$f(w/h_r) = 1.34e^{(-5.46\frac{w}{h_r})}$	0.026	0.19

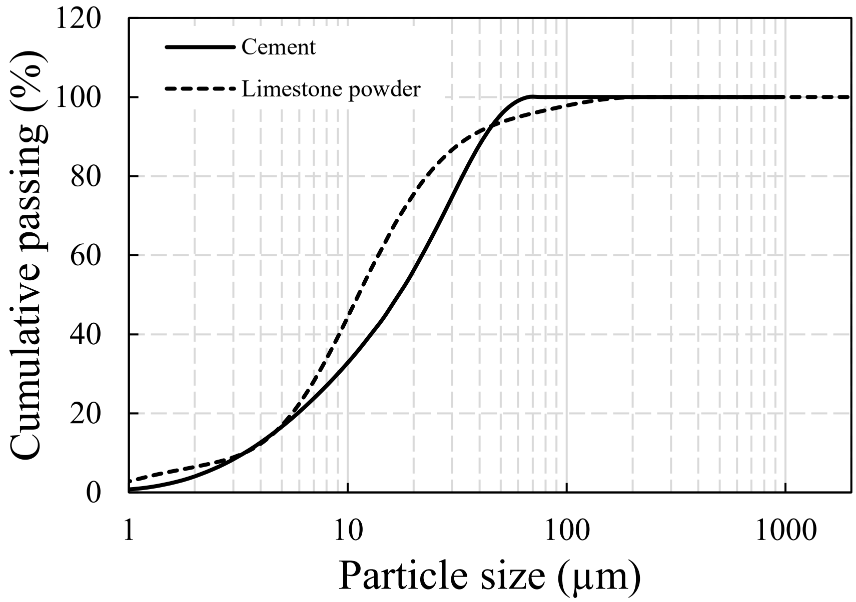

Fig. 1 Particle size distribution of the powders used in the present study

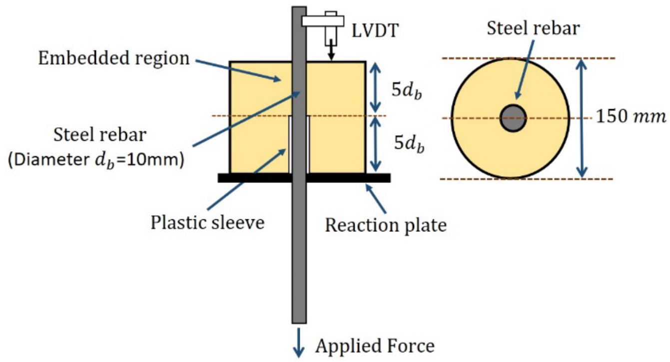

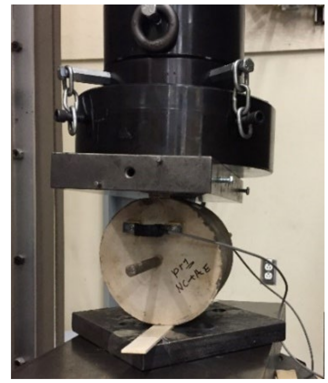

(a) (b)

(c)

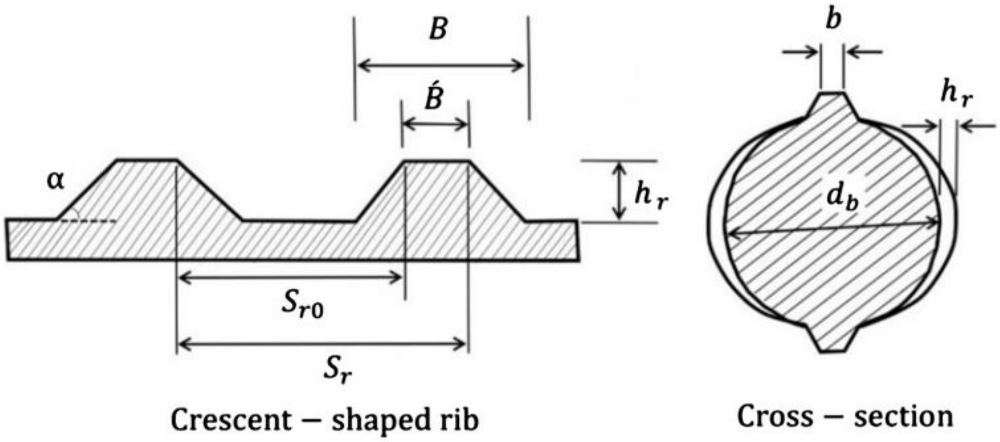

d_b (mm)	h_r (mm)	B (mm)	b (mm)	S_r (mm)	S_{r0} (mm)	α (degree)
10	1.89	4.86	2.70	13.22	12.14	55

(d)

Fig. 2 Test set-up: (a) specimen dimensions and pull-out test setup ; (b) pre-cracking test; (c) pre-cracked specimens; (d) rebar geometry

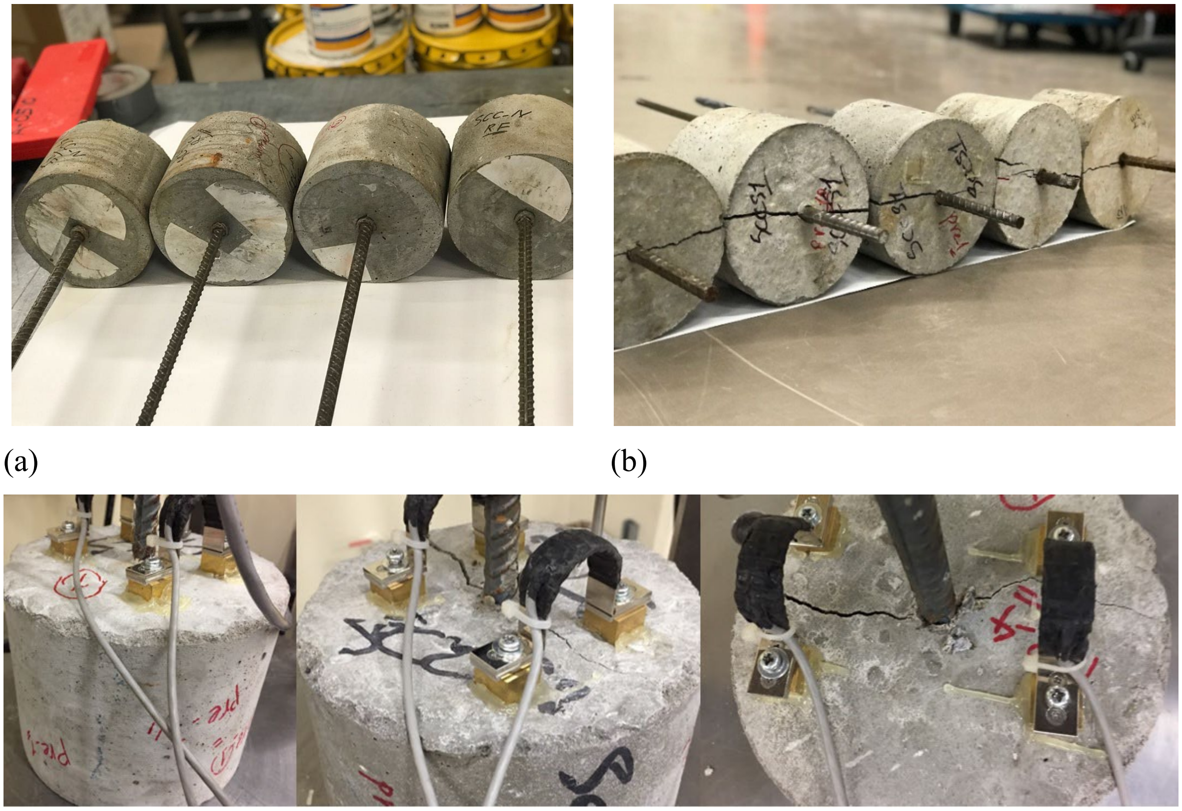

(a) (b)

(c)

Fig. 3 Failure modes: (a) pull-out; (b) splitting; (c) crack opening during pull-out tests

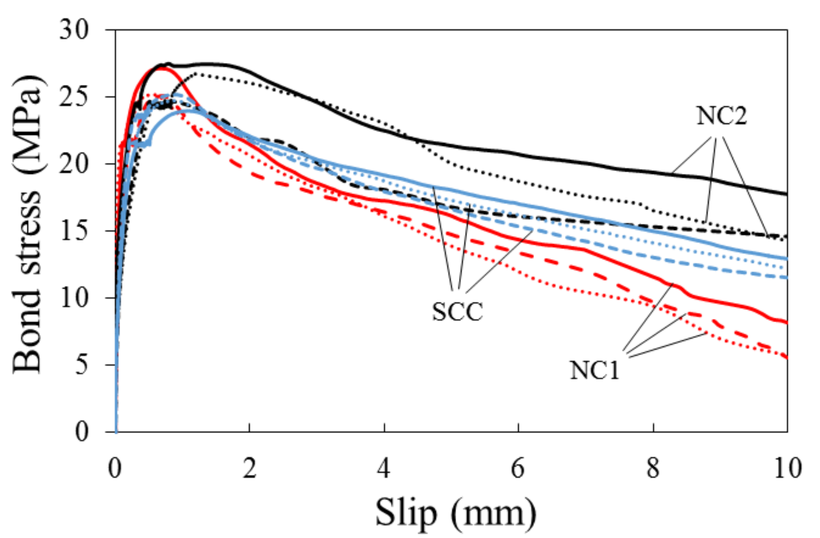

(a)

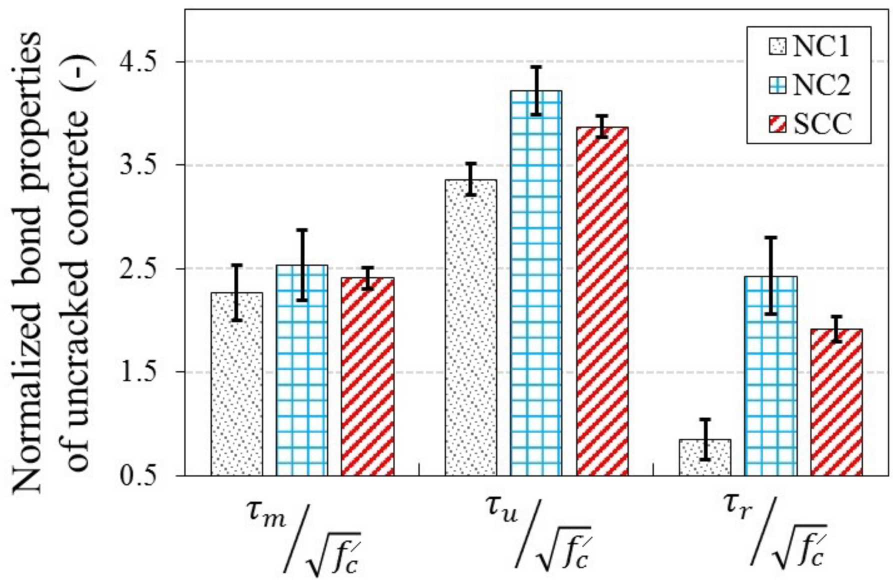

(b)

Fig. 4 Uncracked concrete results: (a) bond-slip curves; (b) normalized bond properties

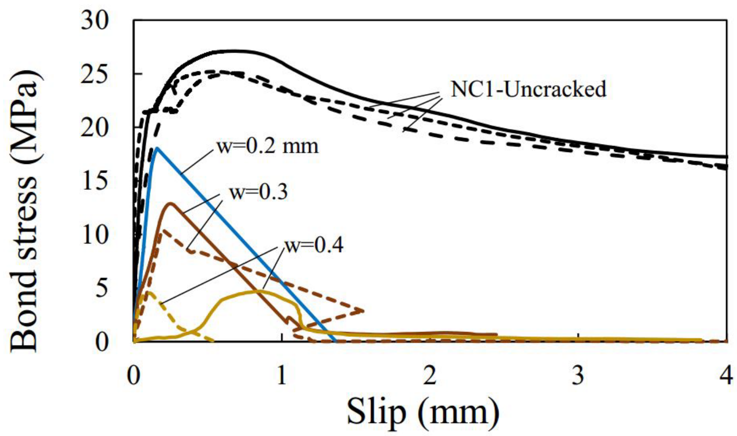

(a)

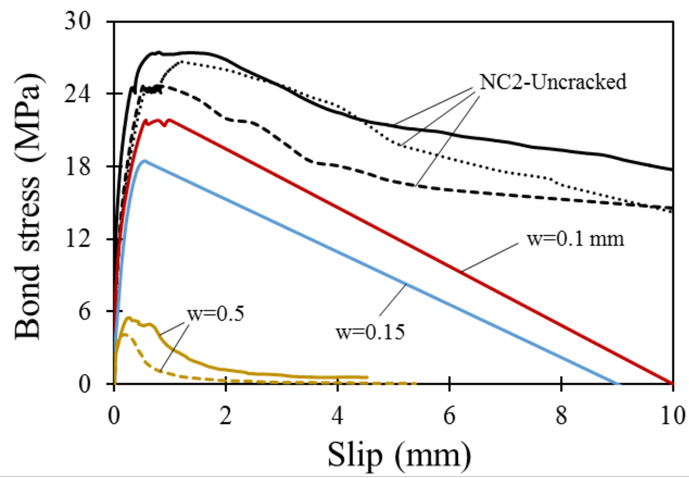

(b)

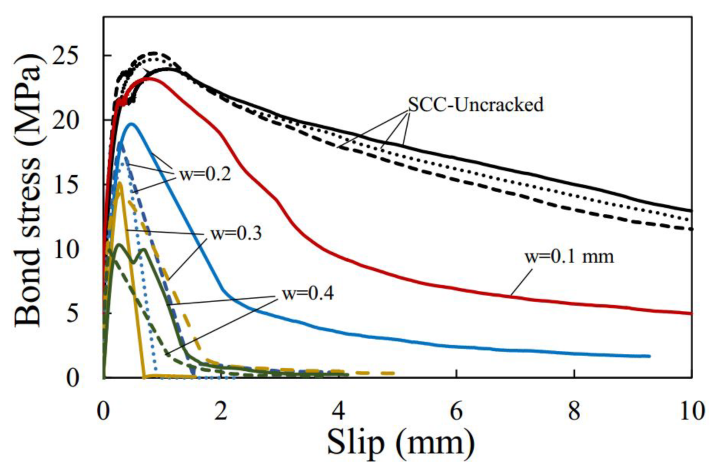

(c)

Fig. 5 Bond-slip responses of uncracked and cracked specimens: (a) NC1; (b) NC2; (c) SCC

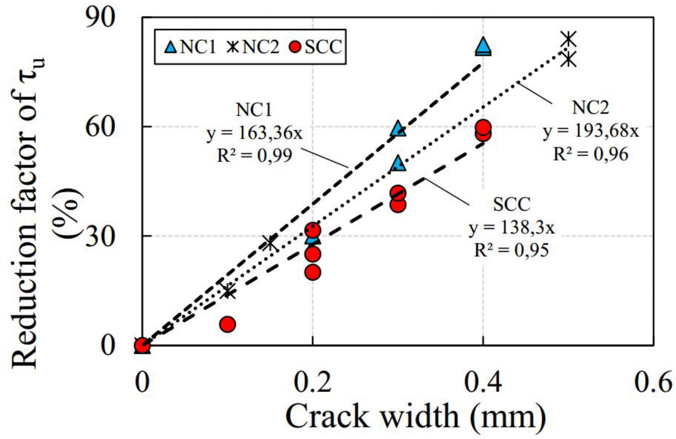

(a)

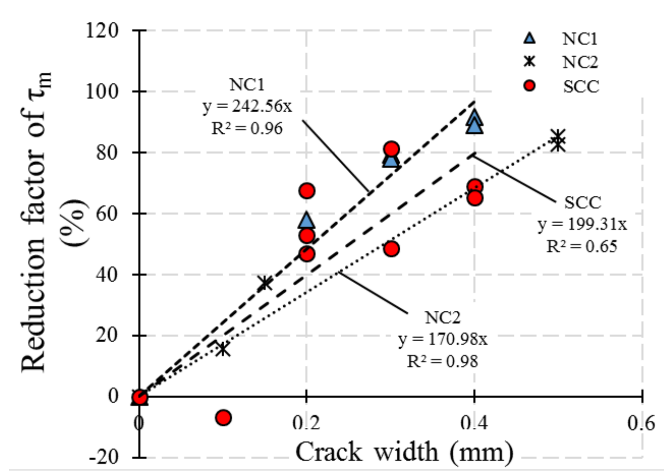

(b)

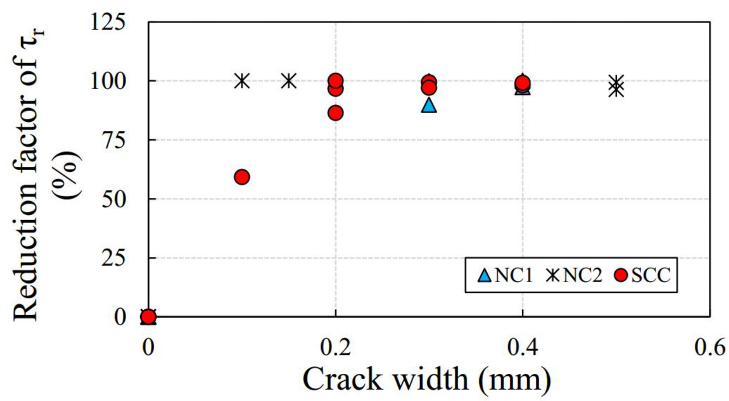

(c)

Fig. 6 Reduction factors of bond response due to the pre-cracking: (a) maximum bond strength; (b) average bond stress; (c) residual bond strength

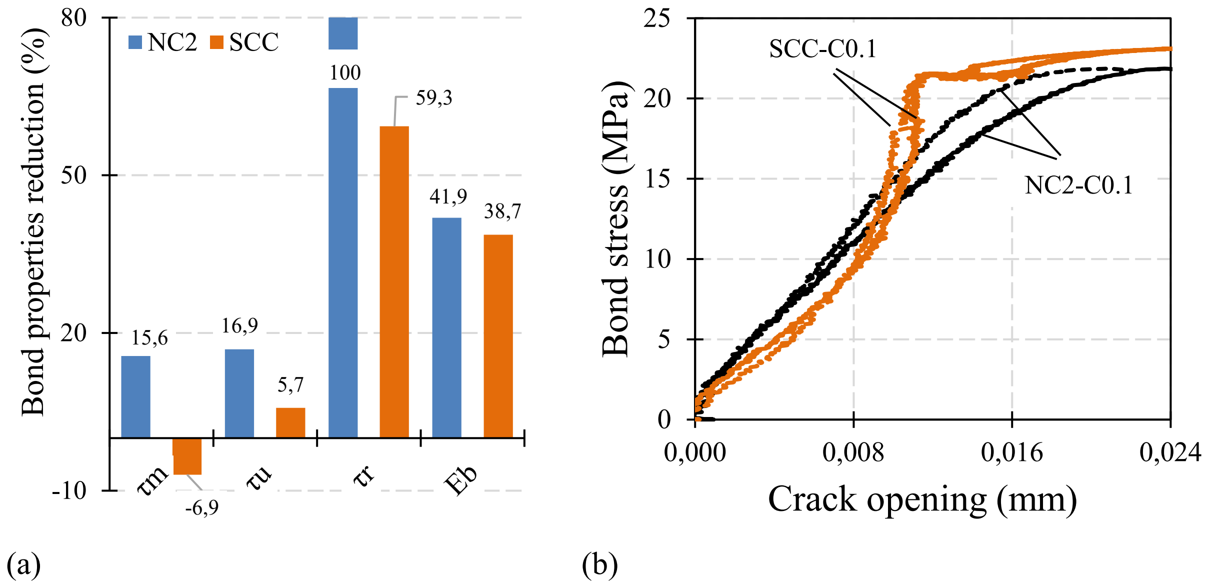

Fig. 7 Effect of small initial crack widths (0.10 mm) on: (a) bond properties; (b) crack opening during pull-out test.

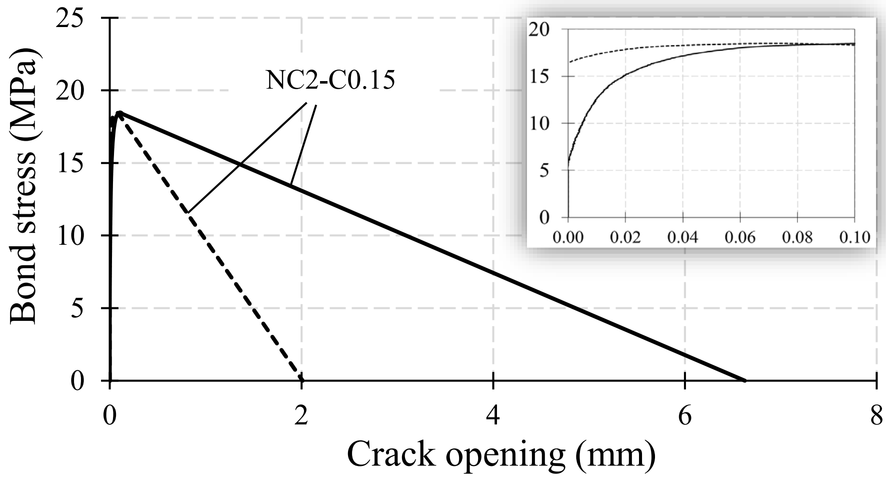
NC2-C0.15
Bond stress (MPa)
Crack opening (mm)

(a)

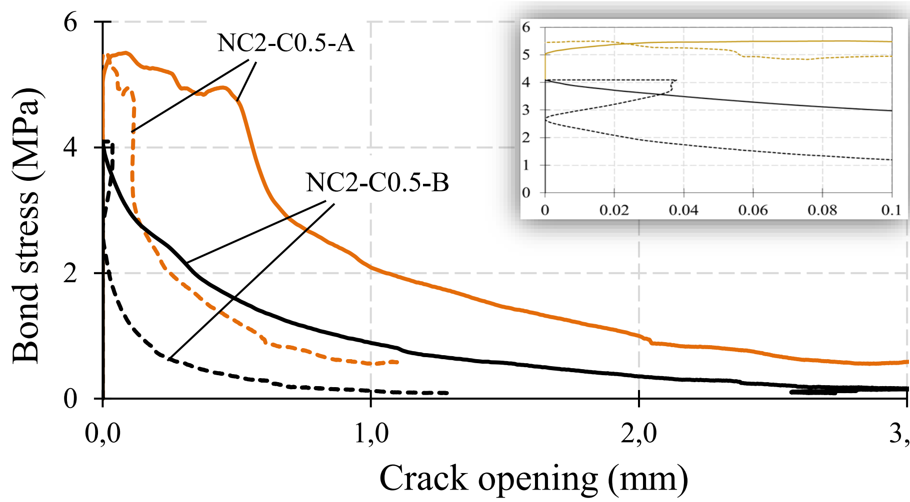
NC2-C0.5-A
NC2-C0.5-B
Bond stress (MPa)
Crack opening (mm)

(b)

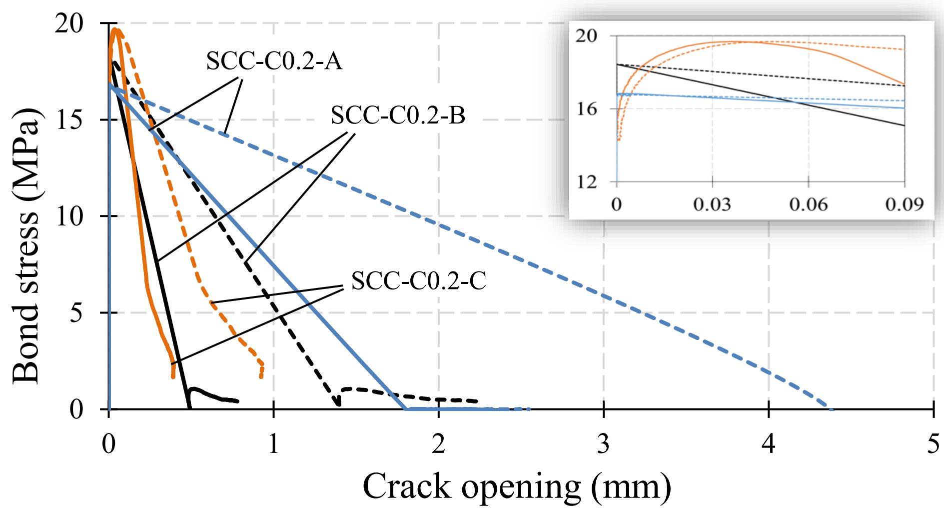
SCC-C0.2-A
SCC-C0.2-B
SCC-C0.2-C
Bond stress (MPa)
Crack opening (mm)

(c)

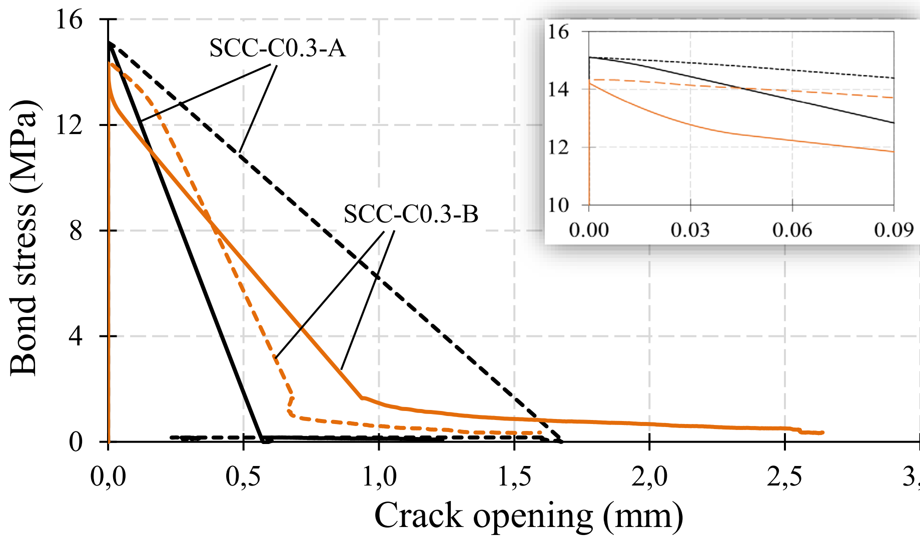

(d)

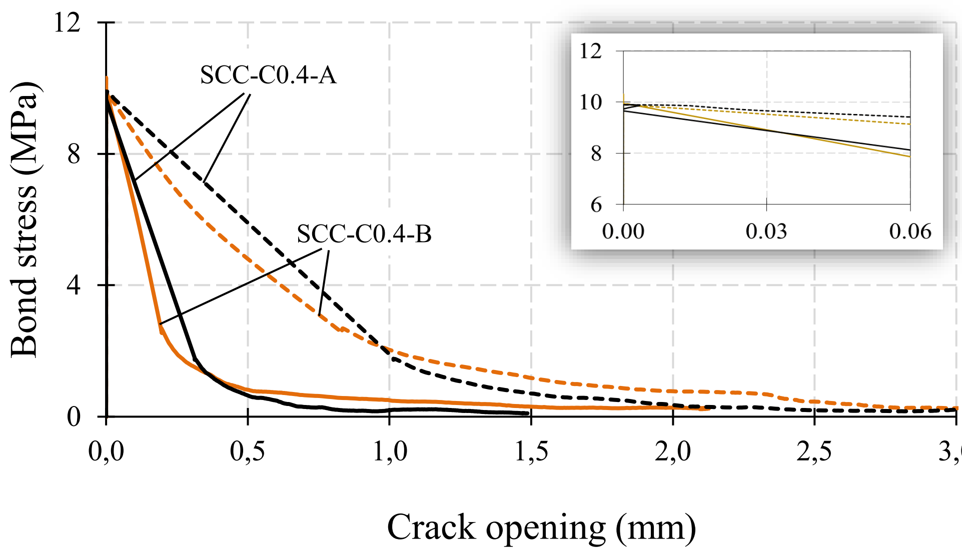

(e)

Fig. 8 Effect of large initial crack widths on bond stress-crack opening curve: (a) NC2 with $w = 0.15$ mm; (b) NC2 with $w = 0.50$ mm; (c) SCC with $w = 0.20$ mm; (d) SCC with $w = 0.30$ mm; (e) SCC with $w = 0.40$ mm

(Note: continuous and dashed lines denote results of crack gauges installed at both sides of rebar during pull-out test)

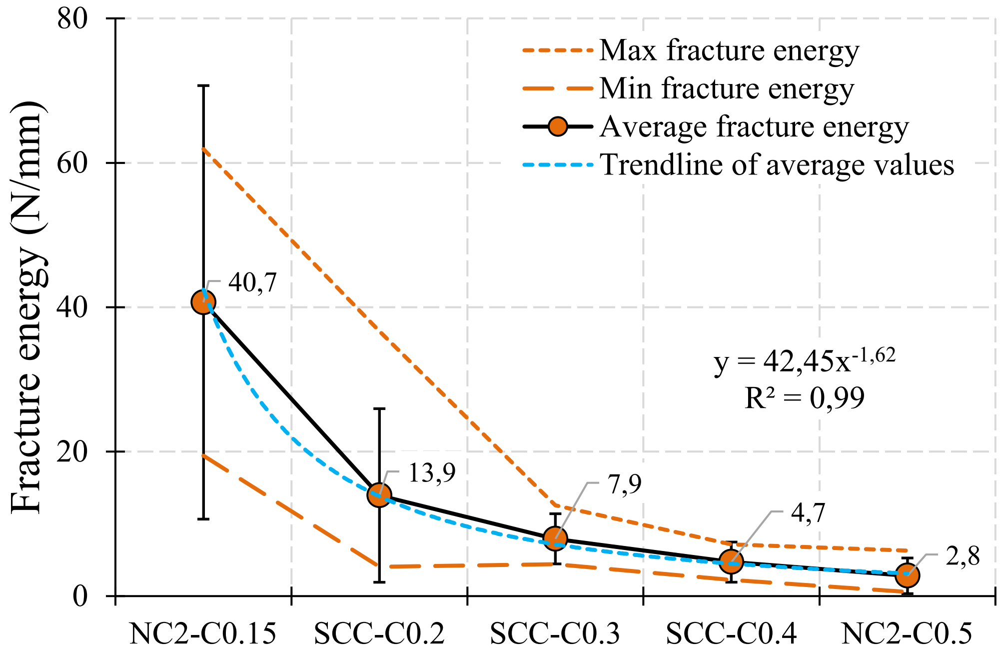

Fig. 9 Fracture energy of cracked specimens from the bond stress-crack opening curve with respect to the initial crack width

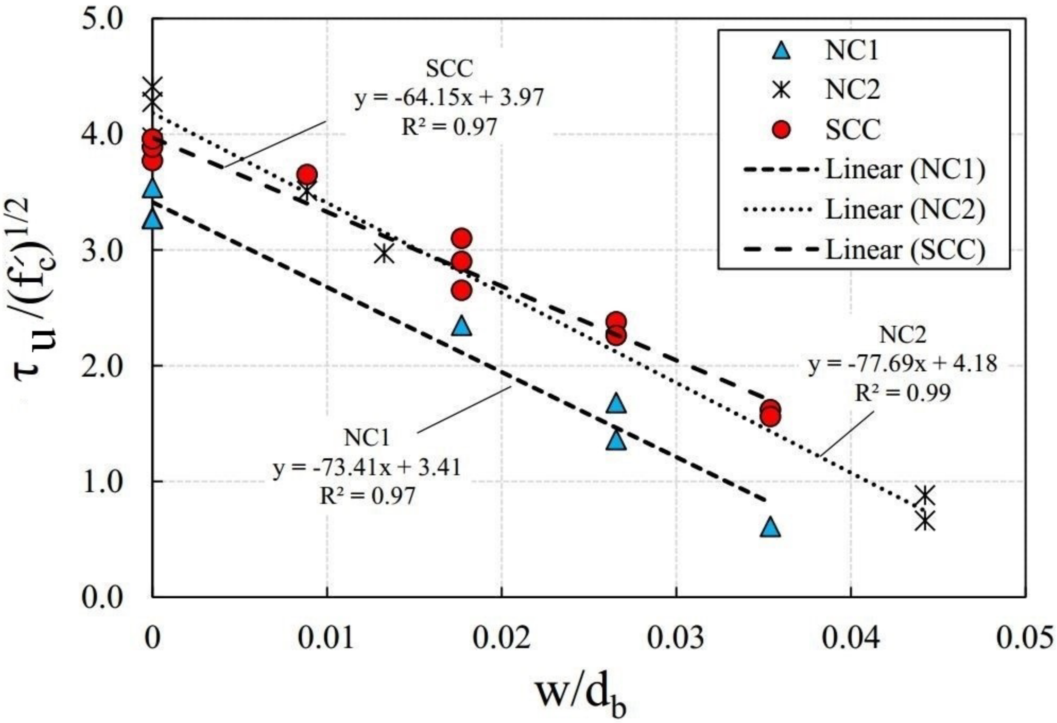

Fig. 10 Correlation of normalized bond strength to w/d_b ratio

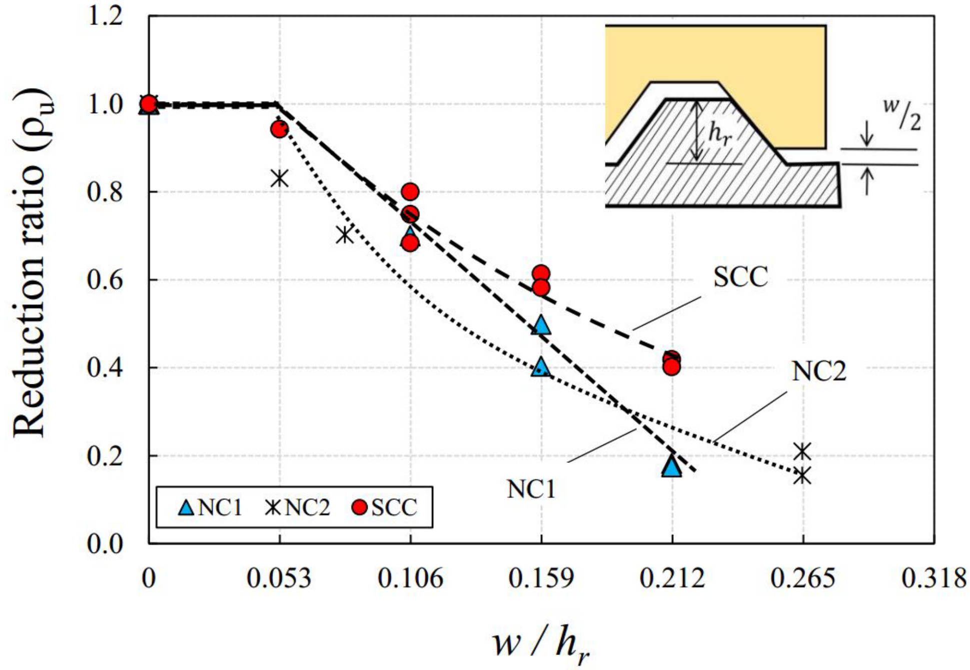

Fig. 11 Reduction ratio of maximum bond strength versus w/h_r ratio for concrete mixtures